

## Electronic Supplementary Information

### A novel hemocompatible core@shell nanosystem for selective targeting and apoptosis induction in cancer cells

*Guillermo Aragonese-Cazorla,<sup>a</sup> Juana Serrano-Lopez,<sup>b</sup> Ines Martinez-Alfonzo,<sup>b</sup>  
María Vallet-Regí,<sup>c,d</sup> Blanca González,<sup>c,d</sup>\* Jose L. Luque-Garcia<sup>a,\*</sup>*

<sup>a</sup> Department of Analytical Chemistry, Faculty of Chemical Sciences, Complutense University of Madrid, 28040, Madrid, Spain.

<sup>b</sup> Experimental Hematology Lab, IIS-Fundación Jiménez Díaz, UAM, Madrid, 28040 Spain.

<sup>c</sup> Department of Chemistry in Pharmaceutical Sciences, Faculty of Pharmacy, Complutense University of Madrid, Instituto de Investigación Sanitaria Hospital 12 de Octubre (i+12), 28040, Madrid, Spain.

<sup>d</sup> Centro de Investigación Biomédica en Red de Bioingeniería, Biomateriales y Nanomedicina (CIBER-BBN), Spain.

\* Corresponding authors.

*E-mail addresses:* [jlluque@ucm.es](mailto:jlluque@ucm.es) (J.L. Luque-Garcia), [blancaortiz@ucm.es](mailto:blancaortiz@ucm.es) (B. González)

## Electronic Supplementary Information

### Table of contents

Characterization techniques (page 2); References of TaqMan gene expression assays used for the RTqPCR analysis (Table S1, page 3); Organic content and elemental composition from thermogravimetric and chemical analysis of Ag@MSNs and functionalized Ag@MSNs materials (Table S2, page 4);  $\zeta$ -Potential values and hydrodynamic particle size in water medium of Ag@MSNs and functionalized Ag@MSNs materials (Table S3, page 5); Fluorescence microscopy image of Ag@MSNs-Tf (Figure S1, page 6); TEM micrograph of Ag@MSNs, histogram of diameters from TEM and polydispersity index (Figure S2, page 7); Powder X-ray diffractogram of Ag@MSNs (Figure S3, page 8); Nitrogen adsorption measurements (Figure S4, page 9); Zeta potential and hydrodynamic size distributions of nanosystems in different media (Figure S5, page 10).

## Characterization techniques

Thermogravimetric analysis (TGA) and differential thermal analysis (DTA) were performed in a Perkin Elmer Pyris Diamond TG/DTA analyser (Perkin Elmer, California, USA) by placing approximately 5 mg of sample in a platinum crucible applying 5 °C/min heating ramps from room temperature to 800 °C under a flow rate of 100 mL/min of air. Chemical microanalyses were performed with a Perkin Elmer 2400 CHN and LECO CHNS-932 thermoanalyzers.

Fourier transformed infrared (FTIR) spectra were collected in a Thermo Nicolet Nexus spectrometer equipped with a Goldengate attenuated total reflectance (ATR) device.

The powder X-ray diffraction (XRD) measurements were performed in a Philips X'Pert diffractometer with Bragg-Brentano geometry operating with Cu K $\alpha$  radiation (wavelength 1.5406 Å) at 40 kV and 20 mA (Philips Electronics NV, Eindhoven, Netherlands). Low-angle XRD patterns were collected in the 2 $\theta$  range between 0.6° and 8° with a step size of 0.02° and contact time of 5 s per step. High-angle XRD patterns were collected in the 2 $\theta$  range between 15° and 100° with a step size of 0.02 s and contact time of 1 s per step.

Transmission Electron Microscopy (TEM) and energy dispersive X-ray spectroscopy (EDS) were carried out with a JEOL JEM 1400 instrument operated at 120 kV (JEOL Ltd., Tokyo, Japan). Sample preparation was performed by dispersing *ca.* 1 mg of sample in 1 mL of water followed by sonication in a low power sonicator bath (Selecta, Spain) for 5 min, and then depositing one drop of the suspension onto carbon-coated copper grids.

The textural properties of the materials were determined by N<sub>2</sub> adsorption porosimetry by using a Micromeritics ASAP 2020 (Micromeritics Co. Norcross, USA). To perform the N<sub>2</sub> measurements, 30 mg of each sample was previously degassed under vacuum for 24 h at 40 °C. The surface area ( $S_{\text{BET}}$ ) was determined using the Brunauer-Emmett-Teller (BET) method and the pore volume ( $V_{\text{p}}$ ) was estimated from the amount of N<sub>2</sub> adsorbed at a relative pressure of 0.98. The pore sized distribution between 0.5 and 40 nm was calculated from the desorption branch of the isotherm by means of the Barrett-Joyner-Halenda (BJH) method and the average mesopore size ( $D_{\text{p}}$ ) was determined from the maximum of the pore size distribution curve.

Electrophoretic mobility measurements for the materials suspended in water were used to calculate the zeta-potential ( $\zeta$ ) values of the nanosystems. Measurements were performed in a Zetasizer Nano ZS (Malvern Instruments Ltd., United Kingdom) equipped with a 633 nm “red” laser. For this purpose, 1 mg of nanoparticles were added to 10 mL of water followed by vortex and ultrasound to get a homogeneous suspension. Measurements were recorded by placing 1 mL of the suspension in a DTS1070 disposable folded capillary cells (Malvern Instruments). The hydrodynamic size of the nanoparticles was measured by dynamic light scattering (DLS) with the same Malvern instrument. Values presented are mean  $\pm$  SD from quintuplicate measurements.

**Table S1.** References of TaqMan gene expression assays used for the RT-qPCR analysis.

<b>Gene</b>	<b>Codified protein</b>	<b>RefSeq</b>	<b>Assay ID</b>
<b>TP53</b>	p53	NM_000546.5	Hs01034249_m1
<b>CDK2</b>	Cdk2	NM_001290230.1	Hs01548893_m1
<b>CCNE1</b>	Cyclin E	NM_001238.3	Hs01026536_m1
<b>CDKN1A</b>	p21	NM_000389.4	Hs00355782_m1
<b>CDK1</b>	Cdk1	NM_001170406.1	Hs00938777_m1
<b>CCNB1</b>	Cyclin B1	NM_031966.3	Hs01030099_m1
<b>CCNA2</b>	Cyclin A	NM_001237.3	Hs00996788_m1
<b>C-MYC</b>	c-Myc	NM_002467.4	Hs00153408_m1
<b>GAPDH</b>	Gapdh	NM_001256799.2	Hs03929097_g1

**Table S2.** Organic content and elemental composition from thermogravimetric and chemical analysis of Ag@MSNs and functionalized Ag@MSNs materials.

Material	Org. Content (wt %)	%C	%N	%S
Ag@MSNs	5.33 <sup>a</sup>	2.13	0.12	0.00
Ag@MSNs-COOH <sub>ext</sub>	6.95 <sup>a,b</sup>	6.53	0.33	0.01
Ag@MSNs-Tf	15.49 <sup>a,b</sup>	11.01	2.08	0.13

<sup>a</sup> Organic content (wt%) is determined from the TGA weight losses, excluding the weight loss due to the desorption of water (up to 125 °C) and <sup>b</sup> further corrected by the weight loss of the remaining alkoxy silanes after the sol-gel reaction (surfactant extracted unmodified Ag@MSNs).

**Table S3.**  $\zeta$ -Potential values and hydrodynamic particle size in water medium of Ag@MSNs and functionalized Ag@MSNs materials.

<b>Material</b>	<b><math>\zeta</math>-Potential <sup>a</sup> (mV)</b>	<b>Hydrodynamic size <sup>a,b</sup> (nm)</b>
<b>Ag@MSNs</b>	$-14 \pm 3$	$68 \pm 6$
<b>Ag@MSNs-COOH<sub>ext</sub></b>	$-26 \pm 6$	$59 \pm 5$
<b>Ag@MSNs-Tf</b>	$-20 \pm 6$	$79 \pm 8$

<sup>a</sup> Samples were measured in quintuplicate (n = 5). <sup>b</sup> Maximum of the size distribution measured by dynamic light scattering.

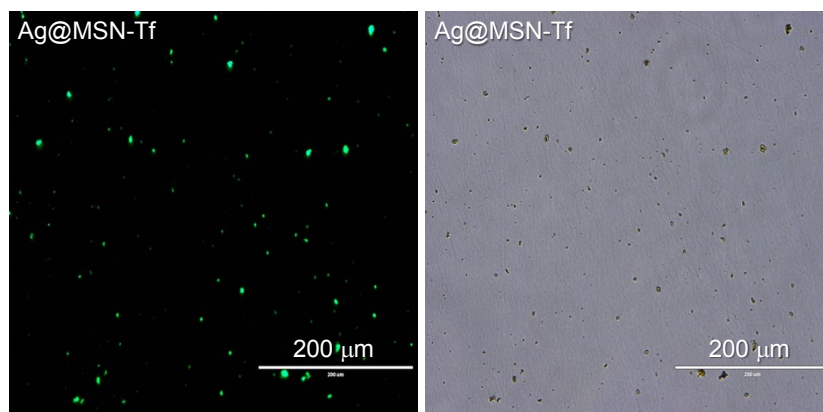


**Figure S1.** Fluorescence microscopy image of Ag@MSNs-Tf nanosystem (left). The bright field image of the same region is shown of the right image. To take the images a suspension of the nanosystem in ethanol is deposited in a well and left to dry before examination under the microscope. Fluorescein green fluorescence from the nanoparticles aggregates, which are formed during solvent evaporation, can be observed.

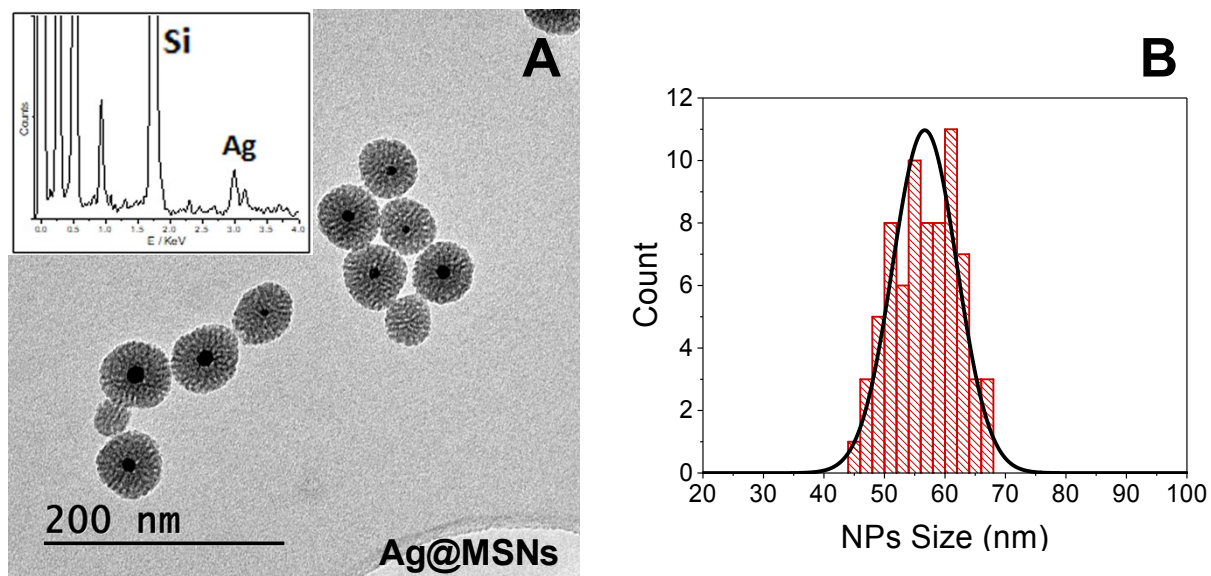


**Figure S2.** A) TEM micrograph of Ag@MSNs, EDS analysis of Ag@MSNs is shown as an inset. B) Histogram of measured nanoparticle diameters ( $n = 73$ ) in the TEM images with the best-fit lognormal distribution superimposed. The normality test using the Kolmogorov-Smirnov approximation gives a p-value of 0.91563, which indicates that at the 0.05 level the data are significantly drawn from a normally distributed population.

The polydispersity index calculated as the square of the relation between the width of the distribution and the mean value of the distribution has a value of 0.138. Therefore, it can be considered that the size distribution of Ag@MSNs nanosystem, with a value less than 0.2 and close to 0.1, tends to be highly monodisperse because a sample is considered monodisperse when the PDI value is less than 0.1.

Nanomaterials for Food Applications - Micro and Nano Technologies, Elsevier 2019, Pages 313-353. Chapter 11 - Characterization of Nanomaterials: Tools and Challenges. T. Mudalige, H. Qu, D. Van Haute, S.M. Ansar, A. Paredes, T. Ingle.

M. Danaei, M. Dehghankhold, S. Ataei, F. Hasanzadeh Davarani, R. Javanmard, A. Dokhani, S. Khorasani, M.R. Mozafari, Impact of Particle Size and Polydispersity Index on the Clinical Applications of Lipidic Nanocarrier Systems, *Pharmaceutics* 2018, **10**, 57.

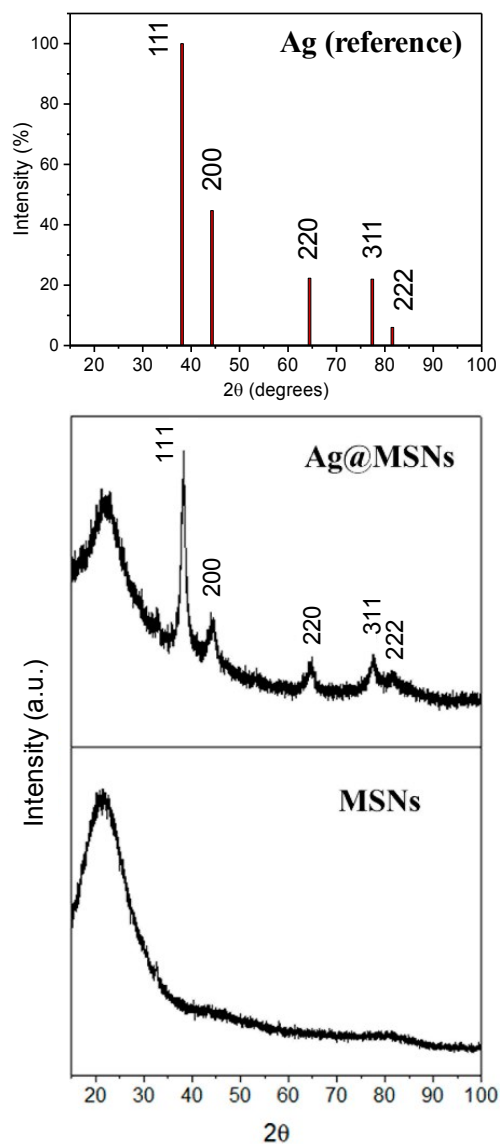


**Figure S3.** A) High angle powder X-ray diffraction pattern of the starting material Ag@MSNs and silver diffraction pattern reference for direct comparison. High angle powder X-ray diffraction pattern of mesoporous silica nanoparticles (MSNs) is also displayed (bottom) to assess that the broad signal appearing between 20 and 30 ° in the diffractogram of Ag@MSNs material is ascribed to the amorphous silica network.



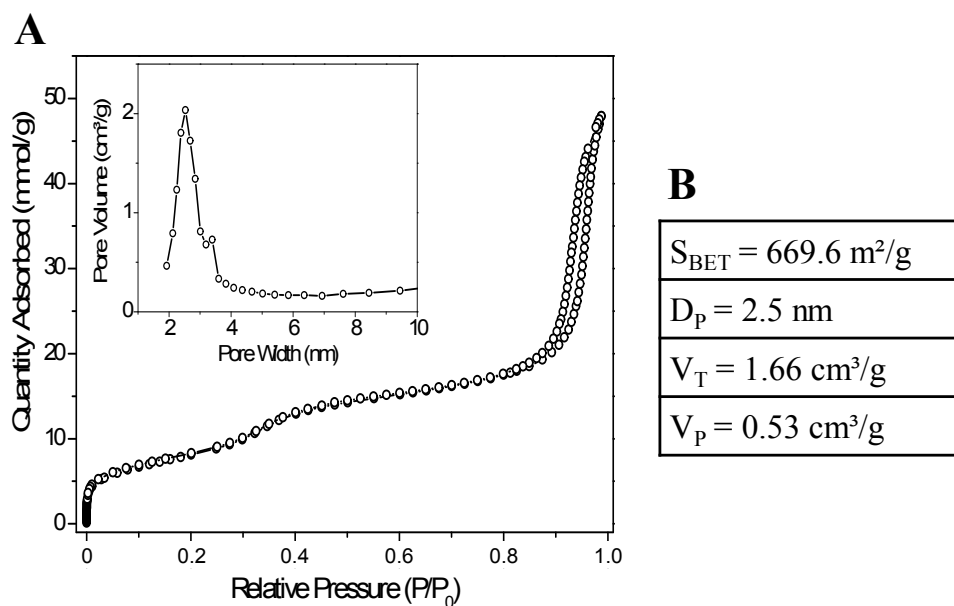


**Figure S4.** A)  $\text{N}_2$  adsorption-desorption isotherms of the Ag@MSN material. Inset: Pore-size distribution for the mesoporous sample. B) Textural parameters of the Ag@MSN material obtained by  $\text{N}_2$  sorption measurements, where  $S_{\text{BET}}$  is the specific surface area obtained by using the BET equation,  $D_{\text{p}}$  is the pore diameter calculated by using the BJH method,  $V_{\text{T}}$  is the total pore volume obtained at  $P/P_0 = 0.99$  and  $V_{\text{p}}$  is the total pore volume obtained at  $P/P_0 = 0.60$ .

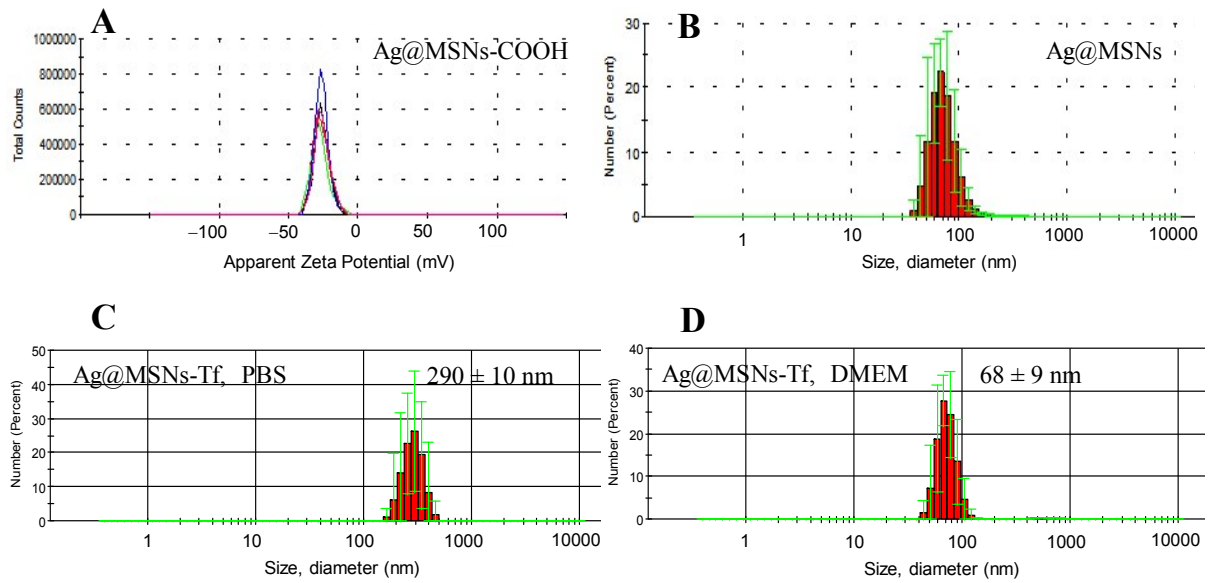


**Figure S5.** A) Zeta potential analysis (five independent measurements) and B) hydrodynamic size distribution obtained by dynamic light scattering of Ag@MSNs-COOH and Ag@MSNs materials suspended in water media as representative examples, respectively. Hydrodynamic size distribution of Ag@MSNs-Tf obtained by dynamic light scattering suspended in PBS (C) and cell culture media DMEM (D).